The Abdus Salam
International Centre for Theoretical Physics

United Nations
Educational, Scientific and
Cultural Organization

IAEA
International Atomic Energy Agency

2152-20

Joint ICTP-IAEA Course on Natural Circulation Phenomena and Passive Safety Systems in Advanced Water Cooled Reactors

17 - 21 May 2010

FLOW STAGNATION AND THERMAL STRATIFICATION IN SINGLE AND TWO-PHASE NATURAL CIRCULATION LOOPS

Jose N. Reyes Jr.
Oregon State University
USA

FLOW STAGNATION AND THERMAL STRATIFICATION IN SINGLE AND TWO-PHASE NATURAL CIRCULATION LOOPS

José N. Reyes, Jr*
Oregon State University, USA

Abstract

The objectives of this lecture are to describe the mechanisms by which natural circulation flow is interrupted in single-phase and two-phase loops and to identify the impact of loop stagnation on thermal stratification within the loop components. By the conclusion of this lecture, the participant should be able to identify the operating conditions that lead to the onset of loop stagnation and the methods that can be used to calculate fluid mixing and plume behavior in the system.

1. INTRODUCTION

This lecture describes the mechanisms that can interrupt natural circulation in loops transporting single and two-phase fluids and the subsequent impact of this stagnation on fluid mixing in the primary loop. The investigation of these mechanisms was conducted in the APEX-CE test facility, at Oregon State University. A schematic of the test facility is shown in Figure 1. APEX-CE was configured to model a 2x4 loop Combustion Engineering PWR. It included the reactor vessel with an electrically heated rod bundle, a pressurizer, two inverted U-tube steam generators, four cold legs and reactor coolant pumps, two hot legs and a safety injection system. The facility had a length scale ratio of approximately 1:4 and a volume ratio of 1:274. It was operated at decay powers ranging down from 6%. Therefore, the tests were conducted after reactor scram with the reactor coolant pumps tripped in a natural circulation mode of operation.

The motivation for the studies in APEX-CE was an issue known as Pressurized Thermal Shock (PTS). In the event of an emergency that results in a significant loss in system pressure or fluid inventory, cold borated water is typically injected into the primary system via the cold legs. If the flow rate in the primary loop is significant, the cold injected fluid will thoroughly mix with the hot water in the primary loop. However, at very low flow rates, the cold injected fluid will stratify in the loops and form cold plumes in the downcomer. Should a pre-existing flaw in the vessel wall or welds exist at a location experiencing prolonged contact with a cold plume, while at high pressure, there is a potential for the flaw to grow into a “through-wall” crack. Sections 2 and 3 describe mechanisms leading to a loss of primary loop flow and Section 4 describes the fundamentals of thermal fluid stratification and plume formation.

* Henry and Janice Schuette Endowed Chair Professor of Nuclear Engineering, Department of Nuclear Engineering and Radiation Health Physics, Oregon State University, Corvallis, Oregon, USA, 97331.

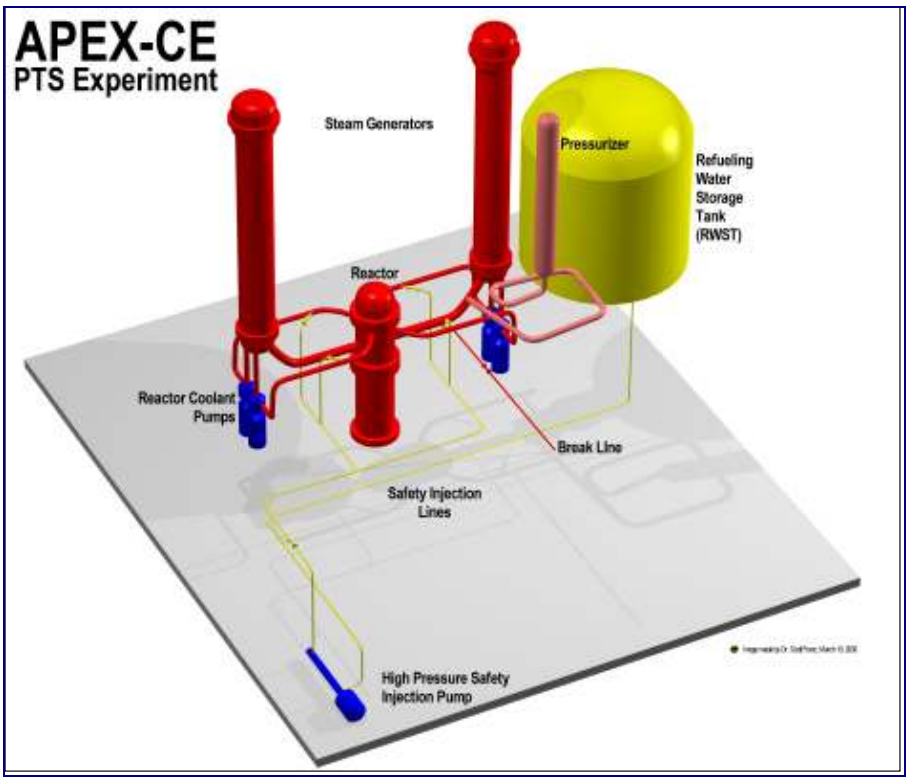

FIG. 1. Schematic of the APEX-CE test facility.

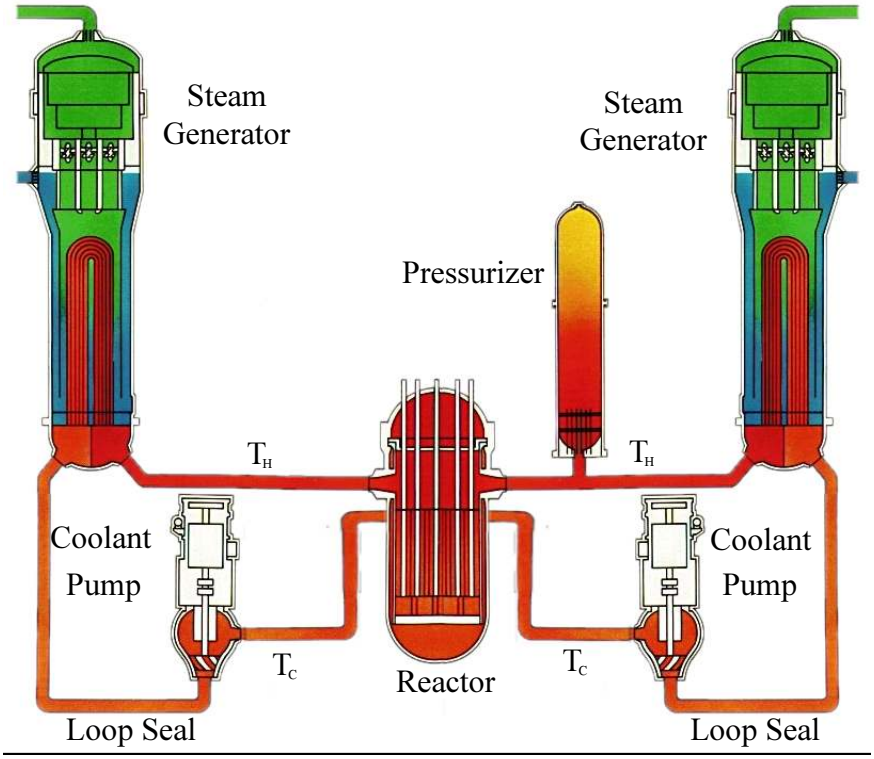

FIG. 2. Control volume for single-phase natural circulation in a two-loop PWR..

2.1. Loss of heat sink (Steam generator reverse heat transfer)

One mechanism for losing single-phase natural circulation flow is a loss of heat sink. This can occur as a result of a loss of main and auxiliary feedwater supplies. This could also occur as a result of a Main Steam Line Break (MSLB) in a single steam generator in a multi-loop plant. In the event of a MSLB, the operators isolate the feedwater to the steam generators and close the main steam isolation valves. This affected steam generator, however, will continue vent steam and depressurize. The blowdown of a steam generator may result in a rapid cooling of the primary system fluid. As a result, the primary loop fluid temperatures may drop below the secondary side temperatures of the "unaffected" steam generators. The result is a loss of heat sink in the loops not experiencing the steam line break. Figure 3 shows that stagnation occurs in cold legs #1 and #3, connected to the unaffected Steam Generator #1 for this test. Figure 4 shows the flow rates for cold leg #1 and #3. When primary side temperature exceeds the secondary side temperature, natural circulation flow is restored.

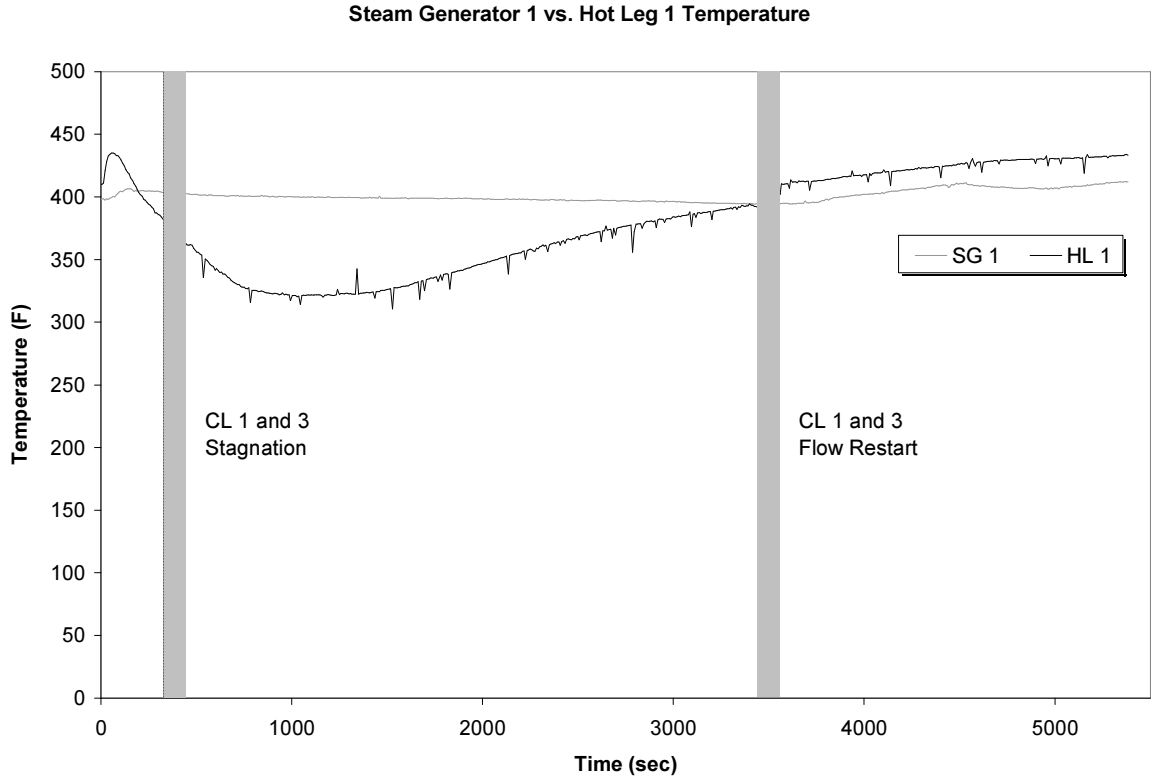

FIG. 3. Illustration of steam generator reverse heat transfer during a main steam line break simulation and recovery (OSU-CE-0012).

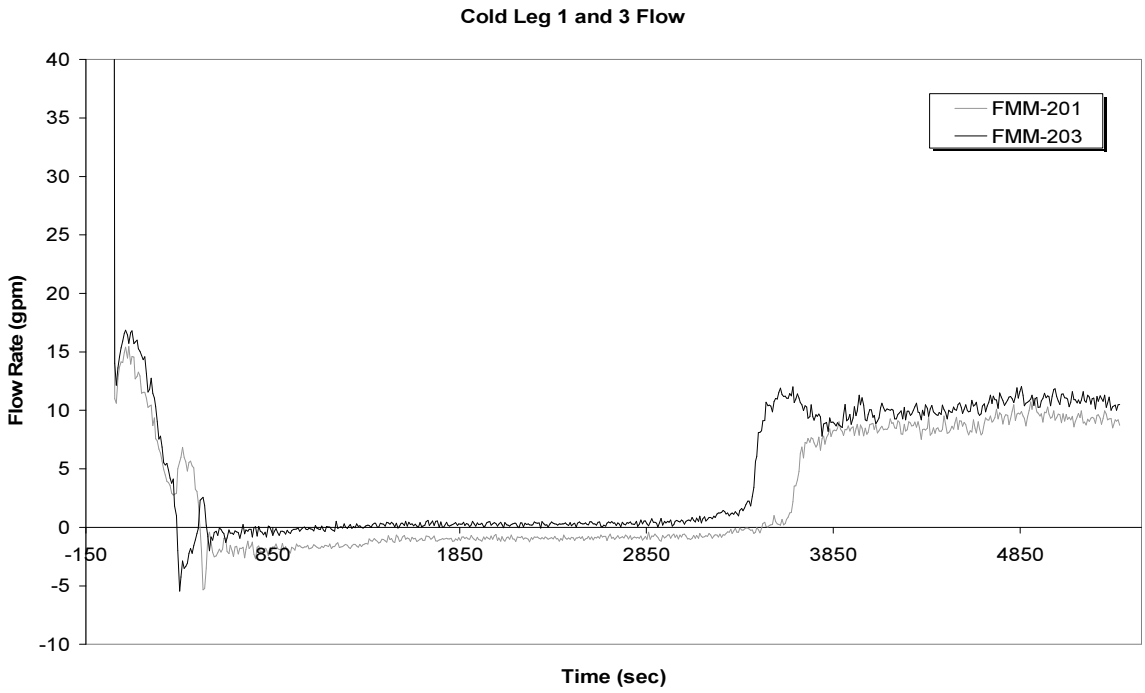

FIG. 4. Illustration of loss of natural circulation flow during a main steam line break simulation and recovery (OSU-CE-0012).

2.2. Negatively buoyant regions in loop (Loop seal cooling)

Another mechanism that can interrupt single-phase natural circulation flow is loop seal cooling. The piping that connects the steam generator lower channel head to the reactor coolant pump is known as the cross-over leg or the reactor pump loop seal as shown in Figure 2. Overcooling transients, such as main steam line breaks, result in a primary side cooldown. If the primary side pressure drops below the safety injection actuation setpoint, cold borated water will be injected into the loop. This water is typically injected into the cold legs of a PWR between the reactor coolant pump and the reactor vessel. Figure 5 is a picture of the transparent Separate Effects Test Loop at Oregon State University used to visualize fluid mixing in a side-injection cold leg.

FIG. 5. Flow visualization of injected coolant mixing with fluid in a transparent loop seal.

The dense injected fluid, simulated using fluorescent salt-water, falls to the bottom of the cold leg where it spreads out towards the vessel and the reactor coolant pump loop seal. Countercurrent flow is established with hot water at the top of the cold leg pipe flowing towards the injection point. The dense injected water mixes with the less dense water in the loop seal creating a negatively buoyant region in the loop, effectively increasing the resistance to flow in that loop. For multi-loop plants, the flow is preferentially diverted to the adjacent cold leg through the SG lower provided the same condition does not also exist there. Figure 6 shows the asymmetric cooling of two loop seals attached to a single steam generator in APEX-CE. Loop seal #4 cools faster than loop seal #2 because the dense fluid back flows over the lip of RCP #4 earlier during this particular transient. Figure 7 shows that loop flow in cold leg #4 stagnates earlier than the flow in cold leg #2.

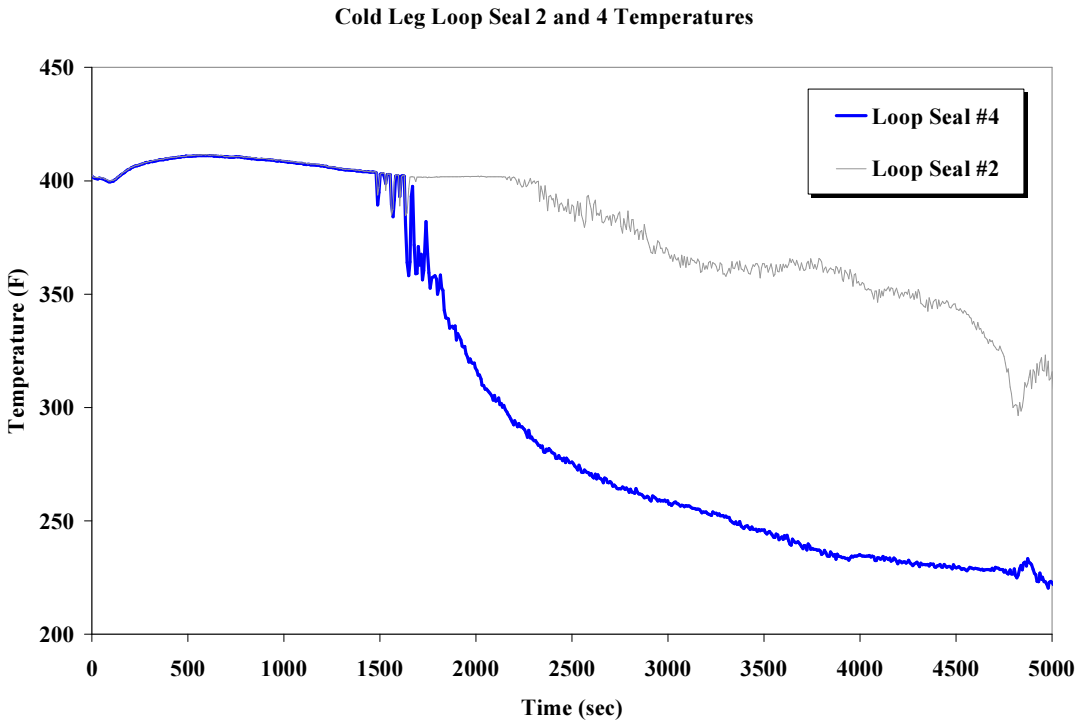

FIG. 6. Asymmetric loop seal cooling (OSU-CE-0008).

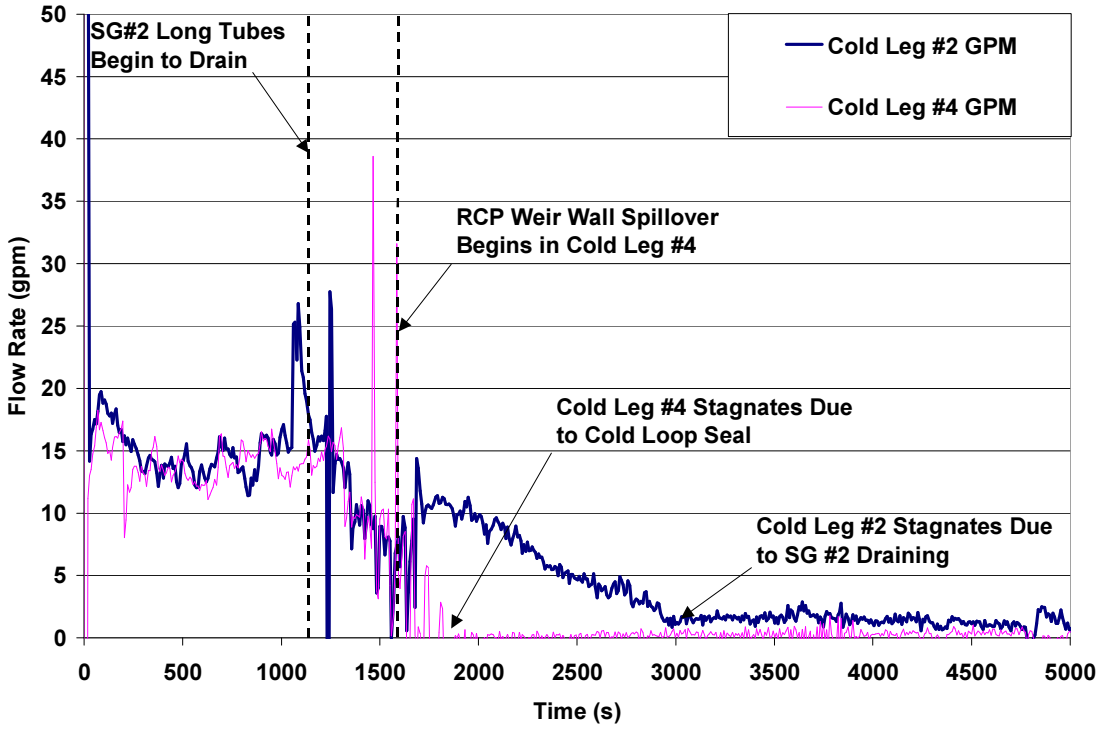

FIG. 7. Stagnation of a primary loop due to loop seal cooling (OSU-CE-0008).

3. TWO-PHASE NATURAL CIRCULATION STAGNATION MECHANISMS

During a Small Break Loss of Coolant Accident (SBLOCA) in a PWR, steam generator tube draining will result in a gradual decrease in primary side natural circulation flow until it transitions to a boiling-condensing mode of operation. Figure 8 shows the results of a test conducted at OSU to investigate this phenomenon. The test, OSU-CE-0002, was a stepped reduction in inventory test. In essence, it is a quasi-steady SBLOCA. It was conducted at a constant core power of 275 kW and initiated from steady-state single-phase natural circulation conditions. A break valve on the reactor vessel was opened to remove primary fluid in stepped intervals. After a short period, the break valve was closed and the loop was allowed to reach a new quasi-steady state flow rate. The cold leg flow rates were measured at each interval. These tests were similar to tests performed at the Semiscale test facility at the Idaho National Engineering Laboratory as shown in Figure 9.[2]

As liquid mass is removed from the system, the loop void fraction increases. This resulted in a rise in the loop flow rates above those observed for single-phase natural circulation as shown in Figure 8. At approximately 70% inventory in APEX-CE, the flow reaches a maximum value. This corresponds to the maximum two-phase buoyancy driving head for the test. Eventually the steam generator tubes begin to drain causing a decrease in flow rate because the distance between the core and steam generator thermal centers has decreased and interruption of flow in the longest tubes**.**

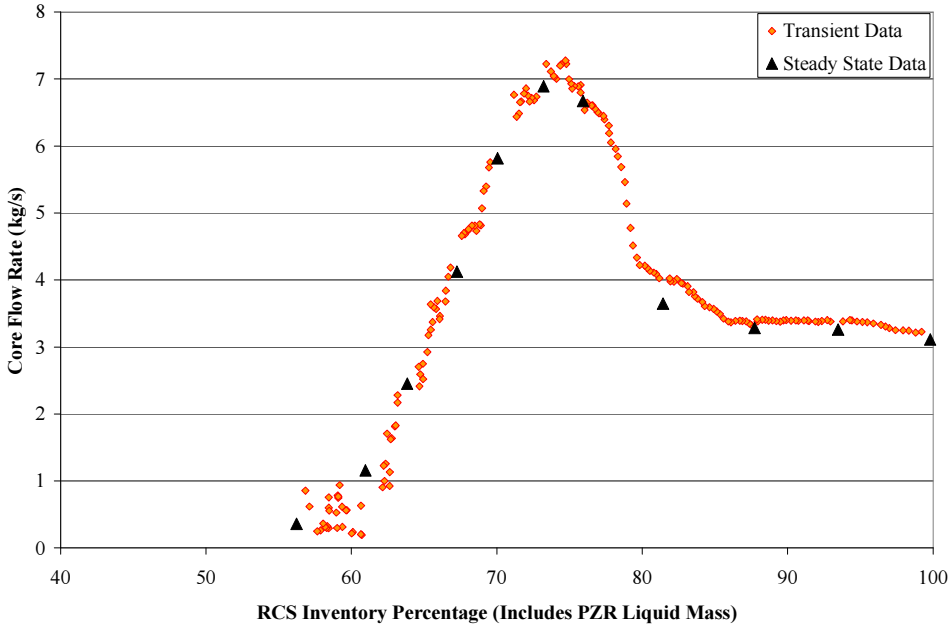

FIG. 8. Cold leg flow rates as a function of primary side inventory during a stepped-inventory reduction test (OSU-CE-0002).

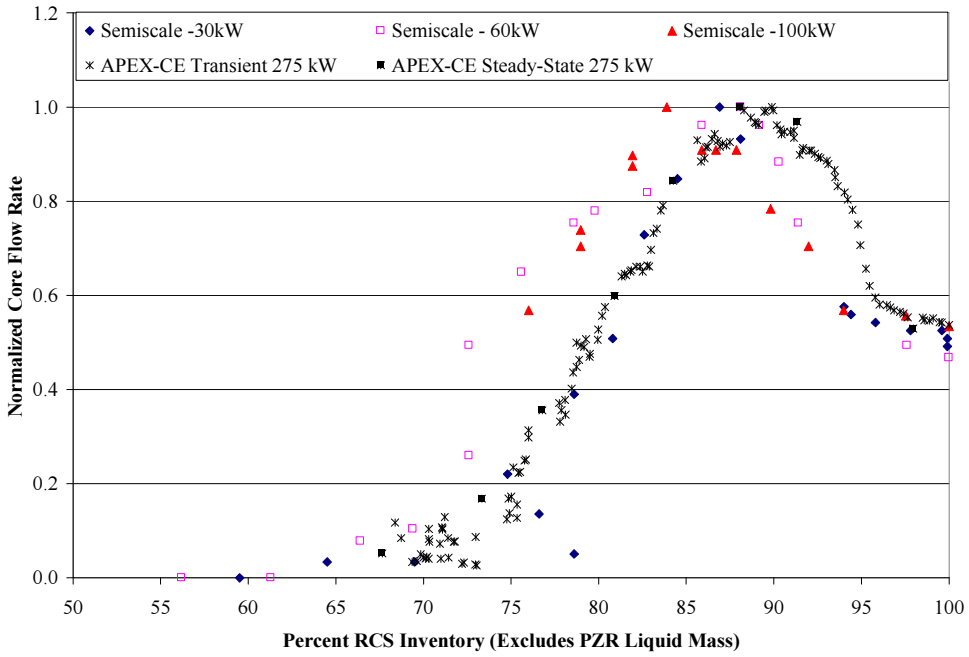

FIG. 9. Cold leg flow rates as a function of primary side inventory during a stepped-inventory reduction test (OSU-CE-0002) and semiscale Mod 2A data.

Figure 10 illustrates the significant difference in draining time for the longest U-tubes at the top of the bundle and the shortest U-tubes at the bottom of the bundle. The long tubes drained much earlier than short tubes. However some primary loop natural circulation continued until the short tubes drained. It is interesting to note that many computer codes typically use one tube to simulate an entire steam generator bundle.

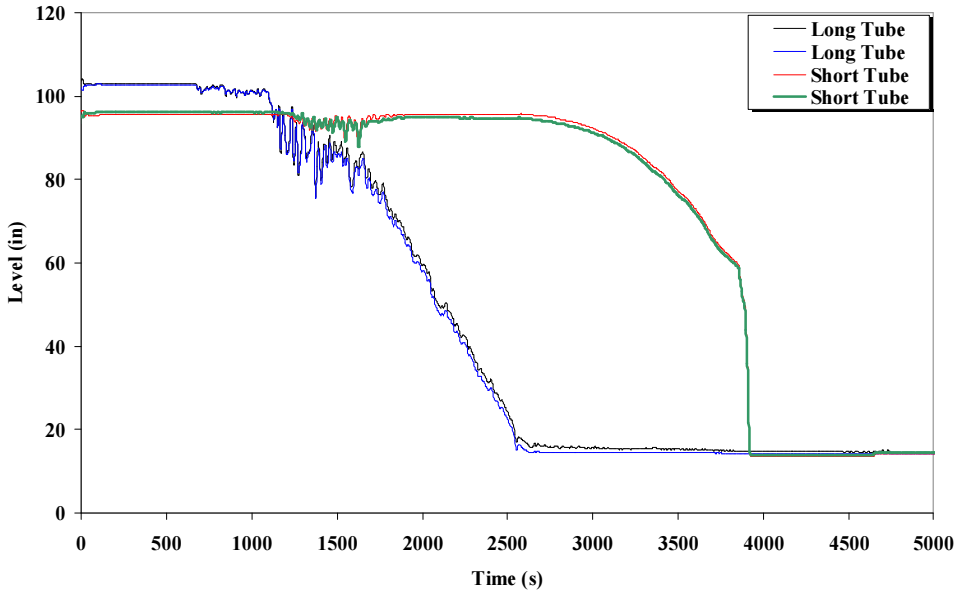

FIG. 10. Liquid levels in the longest and shortest tubes of steam generator #2 during SLOCA test (OSU-CE-0008).

4. THERMAL FLUID STRATIFICATION AND PLUME FORMATION

The loss of natural circulation flow during safety system operation is of particular interest because the flow tends to keep the fluid relatively well mixed in the primary loop. Figure 11 illustrates various regions where thermal stratification can occur.

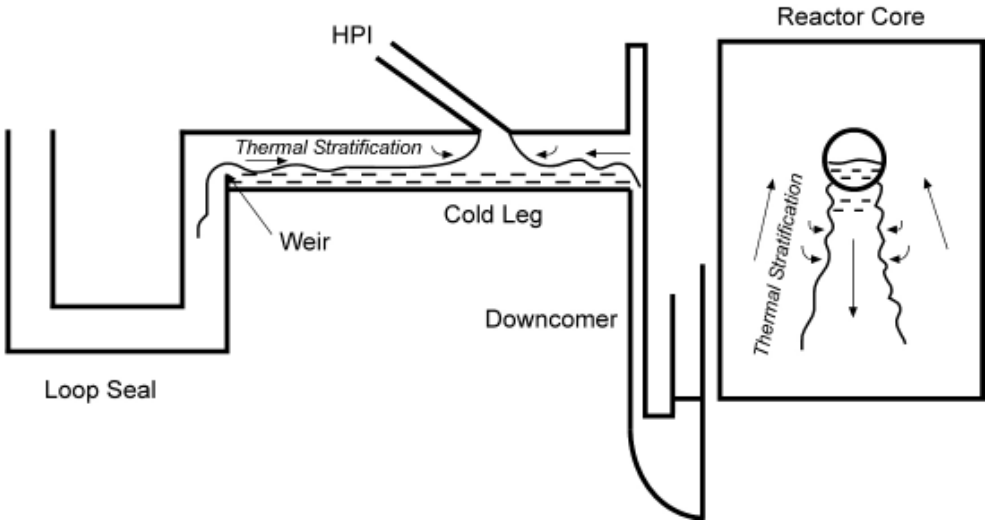

FIG. 11. Regions of thermal stratification in the primary loop of a PWR..

This section presents criteria to predict the onset of thermal stratification in the cold leg and the fundamentals of plume formation in the cold leg and downcomer regions of a reactor vessel.

4.1. Onset of thermal stratification in a horizontal cold leg

Theofanous, et al. (1984) [2], successfully correlated the onset of cold leg thermal stratification for the geometry shown in Figure 11 using the following criterion:

$$Fr_{HPI/CL} = \left[1 + \frac{Q_L}{Q_{HPI}}\right]^{-7/5} \tag{1}$$

where Q_L is the volumetric flow rate through a cold leg, Q_{HPI} is the volumetric flow rate through a single injection nozzle and $Fr_{HPI/CL}$ is a modified Froude number defined as:

$$Fr_{HPI/CL} = \frac{Q_{HPI}}{a_{CL}\left[gD_{CL}\dfrac{\rho_{HPI} - \rho_{CL}}{\rho_{HPI}}\right]^{1/2}} \tag{2}$$

Reyes (2001) [3] developed a criterion similar to that of equation (1) using a hydraulic jump analysis. The criterion is as follows:

$$Fr_{HPI/CL} = \left[1 + \frac{\rho_L Q_{HPI}}{\rho_{HPI} Q_L}\right]^{-1/2} \left[1 + \frac{Q_L}{Q_{HPI}}\right]^{-3/2} \tag{3}$$

As shown in Figure 12, the two criteria given by equations (1) and (3) are similar at the high loop flow to injection flow ratios (i.e., $Q_L/Q_{HPI} >> 1$). The two criteria diverge significantly as Q_L/Q_{HPI} approaches 1.

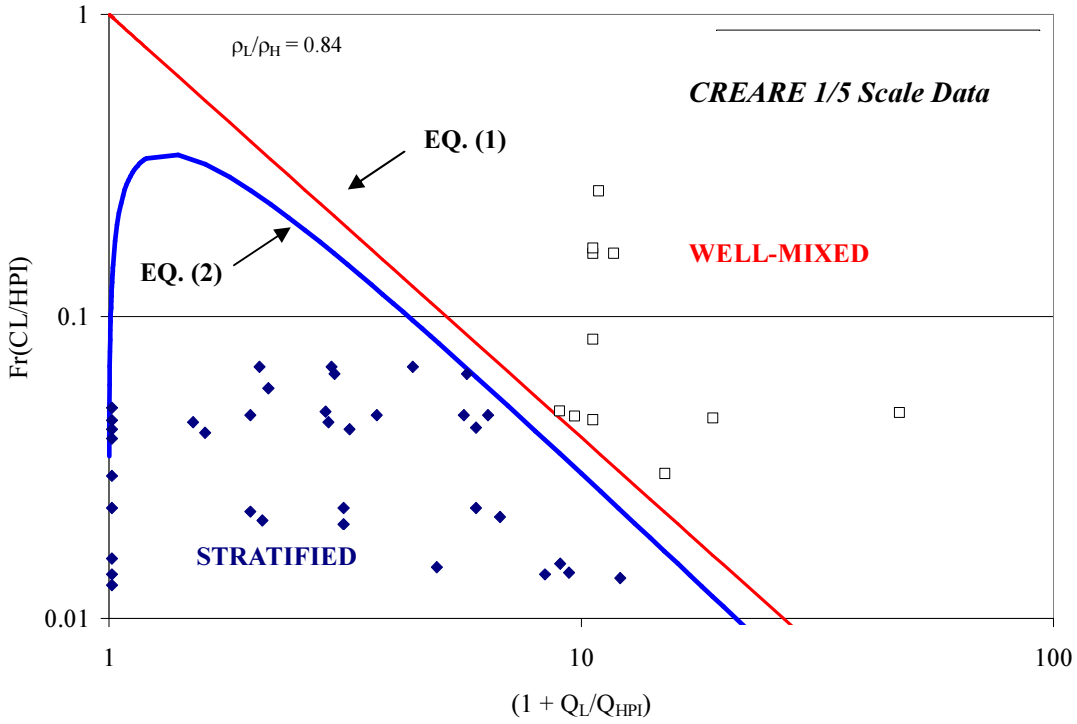

FIG. 12. Comparison of thermal stratification criteria in a horizontal cold leg.

4.2. Governing equations for axisymmetric forced plumes

The criteria of the previous section indicates that upon a loss of natural circulation flow in the loop, (i.e., $Q_L = 0$), the fluid in the cold leg becomes thermally stratified. As illustrated in Figure 13, the cold (approximately 5°C to 20°C) HPI fluid enters the top of the cold leg, creating an axisymmetric plume that falls to the bottom of the pipe. Mixing occurs at the boundary of the HPI plume and at the free shear layers as illustrated in Figure 13. The falling plume produces a head wave that spreads the cold HPI fluid in both directions. After the initial transient, a stagnant pool of HPI fluid forms on the RCP side of the cold leg and all of the HPI flow is directed towards the reactor vessel downcomer. As depicted in this figure, hot water from the loop and downcomer is entrained into the falling plume. This is shown as Region 1 of the figure.

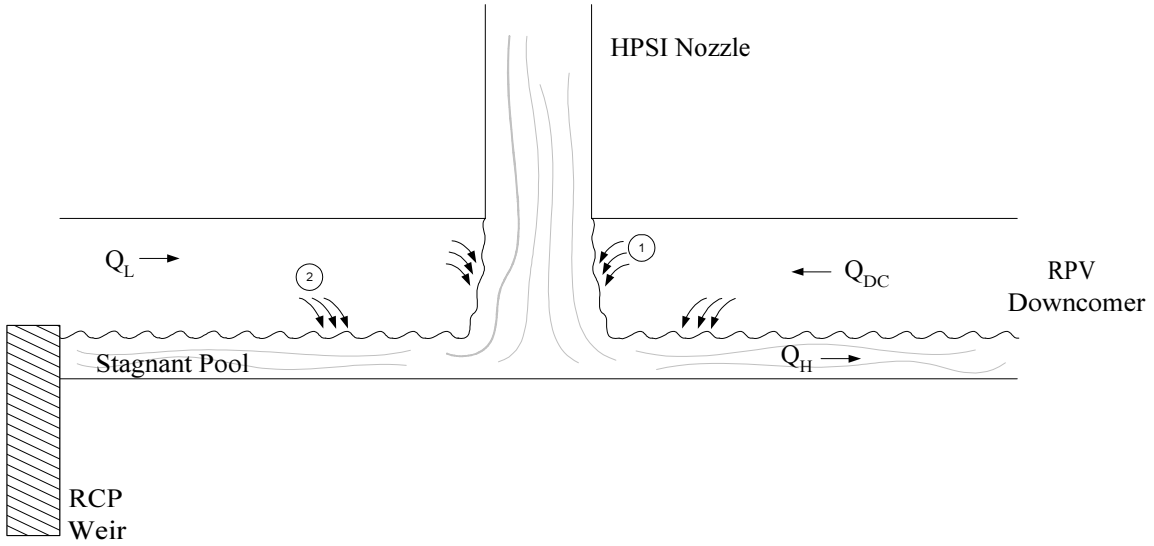

FIG. 13. Thermally stratified conditions for the top-entry HPI..

Mixing also occurs at the free shear layers identified as Region 2 on the figure. Experimental evidence from the CREARE 1/5 [4], CREARE ½ [5] and Purdue ½ [6] scale test facilities indicate that mixing at the free shear layers is negligible compared to plume entrainment mixing. This may not be true for side injection. The focus of this section will be to describe the governing equations for the HPI mixing in Region 1. That is, entrainment mixing of the vertical forced plume and the resulting plume temperature decay.

A. Fundamental Assumptions

Early studies of the behavior of forced plumes relied on similarity solutions derived from the governing conservation equations. Particularly notable in this regard are the works of Rouse, Yih and Humphreys (1952) [7], Batchelor (1954) [8], Morton (1958) [9], and Turner (1979) [10].

Based on Batchelor's work, vorticity, or shearing motion, is generated inside a falling plume as a result of friction at its outer surface. This shearing motion is distributed through the plume by the downward motion along the vertical axis of the plume. The fluid outside the plume will be free from vorticity except in the thin boundary layer near the interface. The turbulent motion inside the plume will produce velocity fluctuations near the interface that will penetrate into the ambient fluid. The plume will break-up only if the inertia of the fluid within the plume is not small compared with the inertia of the fluid surrounding the plume. Therefore, turbulent entrainment of the ambient fluid into the plume, dilution (thermal or solute concentrations) of the density difference and the rate at which the plume falls depends greatly on the ambient fluid density. Further studies by Turner revealed that entrainment takes place in two stages, the engulfing of external fluid by larger eddies at the boundary, followed by rapid, smaller scale, mixing across the central core.

In Morton's analysis of forced plumes, he made three key assumptions that enabled him to obtain solutions to the governing conservation equations. These assumptions are described in the following paragraphs.

i. Taylor's Entrainment Assumption

G.I. Taylor [11] was the first to recognize that the linear spread of the plume radius with axial position implies that the mean inflow velocity across the edge of the plume is proportional to the local mean downward velocity of the plume. That is,

$$-v_E = \alpha_E u_p \tag{1}$$

Where the ratio of the mean speed of inflow v_E at the edge of the forced plume to the mean vertical speed on the plume axis, u_p is equal to an entrainment constant, α_E, which is a value between zero and one. Taylor's assumption of a constant value of α_E is known to be true for pure plumes or pure jets. Other correlations for α_E have been developed for forced plumes in which both the momentum flux and buoyancy flux are important.

ii Similarity of Velocity and Buoyancy Profiles

Morton assumed that the profiles of mean vertical velocity and buoyancy are each of similar form at all axial elevations. The experimental data strongly supports this assumption as shown in Figure 14, which is a plot of the local velocity inside a planar plume. Figure 15 demonstrates that all of the data collapses to a single curve when plotted in dimensionless coordinates.

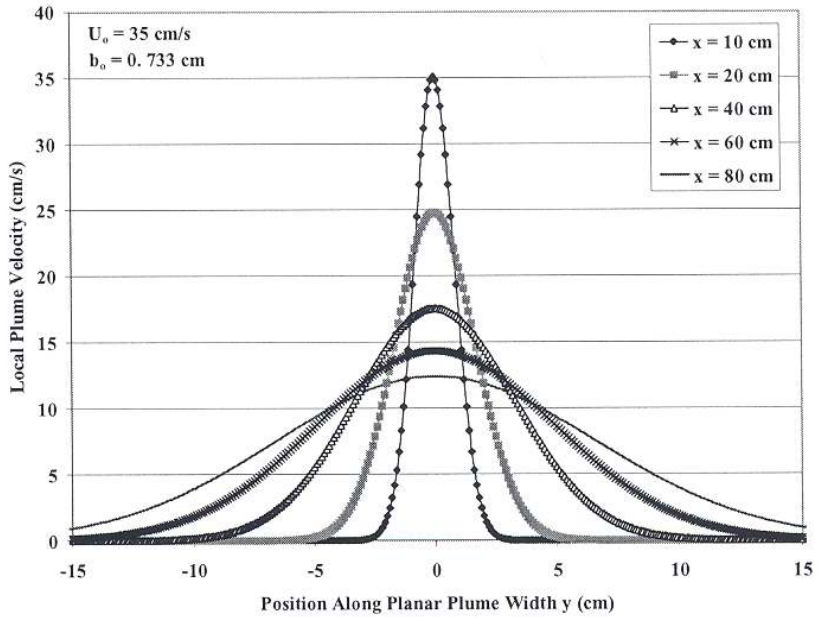

FIG. 14. Correlation of velocity distributions measured in a planar jet (1934) [12]

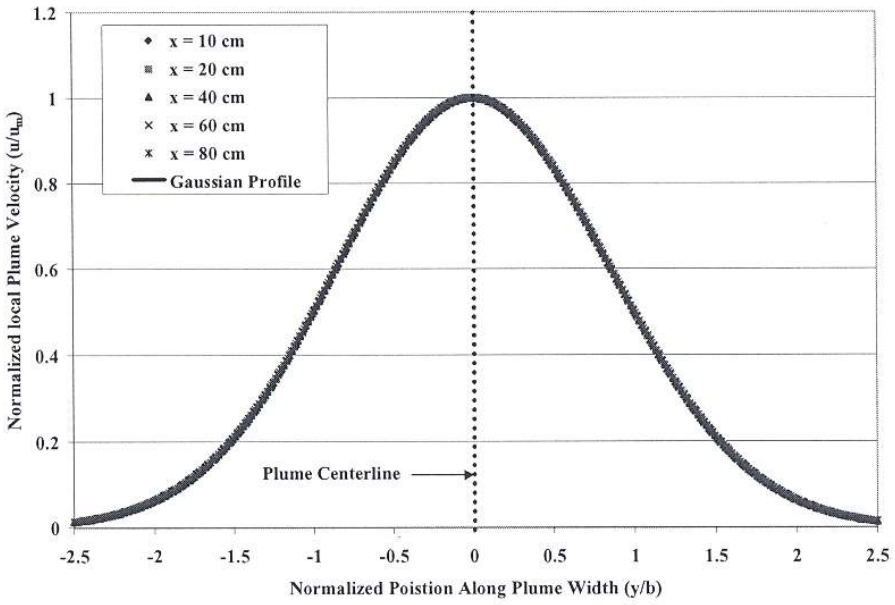

FIG. 15. Velocity distributions in a planar jet plotted in dimensionless Coordinates [12] and compared to a gaussian profile (1934).

By assuming a particular profile shape, typically a Gaussian profile as shown in Figure 15, the mass and momentum fluxes can be replaced by mean value defined by integrals across the plume width. The assumption of similarity implies that the rate of spread of the plume, which is governed by the turbulence generated by its own motion, must have the same relation to the mean flow whatever the scale of motion.

i. Gaussian Profile

The following Gaussian profiles are typically assumed for the mean vertical velocity and mean buoyancy respectively.

$$u(r,z) = u_p(z)\exp\left(-\frac{r^2}{b_u^2}\right) \tag{2}$$

and

$$g\Delta\rho(r,z) = g\Delta\rho_p(z)\exp\left(-\frac{r^2}{b_u^2}\right) \tag{3}$$

where

$$\Delta\rho = (\rho - \rho_m) \tag{4}$$

In these profiles, u_p and $g\Delta\rho_p$ are the mean axial velocity and buoyancy of the forced plume. These mean values are functions of the axial position (z). The ambient fluid density is denoted by ρ_m. The profile dependence on the radial position is given by the r-coordinate found in the exponent. The length b_u characterizes the radial spread of the velocity profiles whereas the length b_g characterizes the radial spread of the buoyancy profile. Both are functions of axial position. The values of b_u and b_g are empirically determined. Figure 16 illustrates the profile nomenclature that has been implemented in this analysis.

The following equation of state for the fluid:

$$\left(T - T_m\right) = \frac{\left(\rho - \rho_m\right)}{\beta_o \rho_o} \tag{5}$$

where β_o is the reference thermal expansion coefficient and ρ_o is a reference density, can be applied to the buoyancy profile to obtain the following fluid temperature profile:

$$\left(T - T_m\right) = \left(T - T_m\right)_p \exp\left(-\frac{r^2}{b_g^2}\right) \tag{6}$$

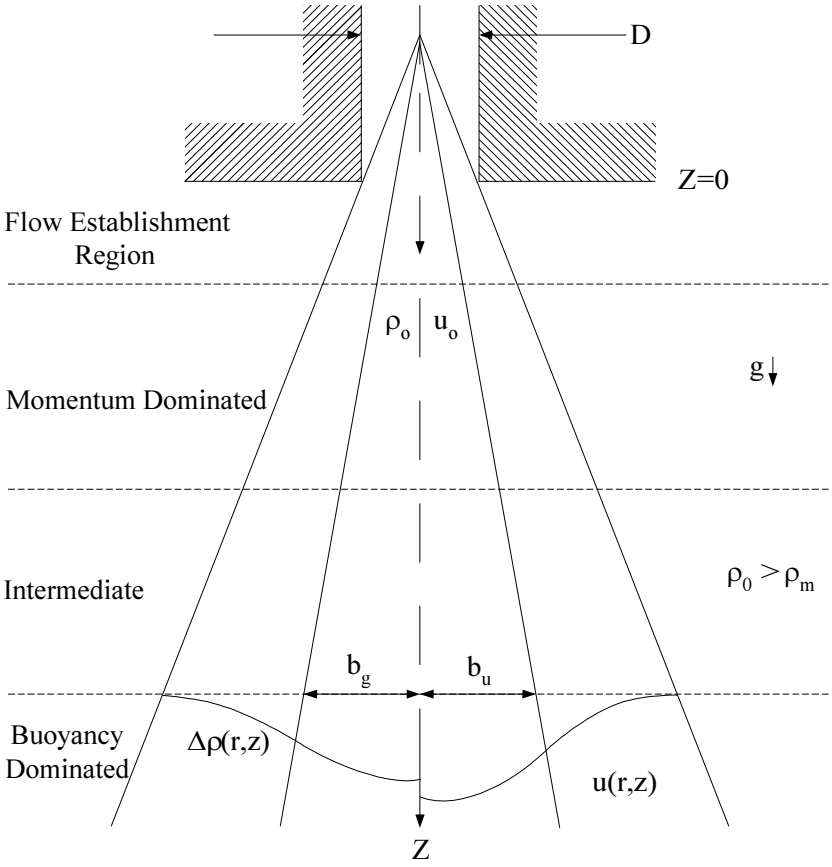

FIG. 16. Gaussian profiles in forced plumes.

B. Governing Equations for Axisymmetric Forced Plumes

The governing equations for the flow quantities in an axisymmetric vertical buoyant jet, where gravity acts along the z-coordinate, are as follows (Chen and Rodi) [13]:

Mass Conservation:

$$\frac{\partial}{\partial z}(\rho u r)+\frac{\partial}{\partial r}(\rho v r)=0 \tag{7}$$

Momentum Conservation:

$$\frac{\partial}{\partial z}(\rho u^2 r)+\frac{\partial}{\partial r}(\rho u v r)=g(\rho-\rho_m)r-\frac{\partial}{\partial r}(r\rho u'v') \tag{8}$$

Thermal Energy Conservation:

$$\frac{\partial}{\partial z}(\rho u T r)+\frac{\partial}{\partial r}(\rho v T r)=-\frac{\partial}{\partial r}(r\rho v'T) \tag{9}$$

The equations listed above were obtained by Chen and Rodi using the boundary-layer assumptions and the Boussinesq approximation under steady-flow conditions. The $\rho u'v'$ term represents the turbulent shear stress. The thermal energy equation can also be written in terms of a stratified ambient temperature, $T_m(z)$ as follows:

$$\frac{\partial}{\partial z}\left[\rho u r(T-T_m)\right]+\frac{\partial}{\partial r}\left[\rho v r(T-T_m)\right]=-\rho u r\frac{\partial T_m}{\partial z}-\frac{\partial}{\partial r}(\rho v' r T') \tag{10}$$

Integrating the mass conservation equation yields the following balance equation for the plume volume flux:

$$\frac{d}{dz}\int_0^R u r dr=-v_E R \tag{11}$$

Where 2π and ρ (Boussinesq approximation) were canceled from both sides of the equation. In this equation, v_E is the entrainment velocity at the plume boundary.

Integrating the momentum conservation equation yields the following balance equation for the momentum flux**:**

$$\frac{d}{dz}\int_0^R \rho u^2 dr=g\int_0^R(\rho-\rho_m)r dr \tag{12}$$

A value of 2π was canceled from both sides of the equation. In arriving at this equation, it was assumed that the terms u and $\rho u'v'$ are close to zero at r equal to R.

Integrating the energy conservation equation yields the following balance equation for the thermal energy flux:

$$\frac{d}{dz}\int_0^R u(T-T_m)rdr = -\frac{dT_m}{dz}\int_0^R urdr \tag{13}$$

The terms 2π and ρ (Boussinesq approximation) were canceled from both sides of the equation. Use has also been made of the approximation that u, $(T-T_m)$, and $\rho v'T'$ are zero at r equal to R.

The integral volume flux, momentum flux, and thermal energy flux equations can be evaluated by substituting the Gaussian profiles presented earlier. This will yield a set of ordinary differential equations which can be made dimensionless to obtain the desired scaling groups. Substituting equation (2) into (11) and performing the integration yields the balance equation for the volume flux**:**

$$\frac{d}{dz}\left(b_u^2 u_p\right) = -2Rv_E \tag{14}$$

Use has been made of the fact that $\exp\left(-R/b_u^2\right)$ is approximately zero. Substituting equation (3) into (10) and performing the integration yields the balance equation for the momentum flux:

$$\frac{d}{dz}\left(\rho b_u^2 u_p^2\right) = 2g\left(\rho-\rho_L\right)_p b_g^2 \tag{15}$$

Substituting equation (6) into (13) and integrating yields the thermal energy flux balance equation:

$$\frac{d}{dz}\left(\frac{b_g^2 b_u^2 u_p \Delta T_p}{b_g^2+b_u^2}\right) = -b_u^2 u_p \frac{dT_m}{dz} \tag{16}$$

Equations (14) through (16) are similar to those obtained by Rodi [14]. The integrated balance equations given by (14) through (16) can also be written in terms of volumetric flow rates, Q. The volumetric flow rate of the plume, Q_p is given by:

$$Q_p = 2\pi\int_0^R urdr \tag{17}$$

Substituting the Gaussian velocity profile, equation (2) and integrating yields:

$$Q_p = \pi b_u^2 u_m \tag{18}$$

The entrainment volumetric flow rate can be related to the entrainment velocity by:

$$\frac{dQ_p}{dz} = 2\pi R v_E \tag{19}$$

Substituting equations (18) and (19) into (14) through (16) yields the governing equations for a forced axisymmetric plume as shown in Table 1. At z = 0, Q_{HPI} is approximately equal to Q_p, D_{HPI} is approximately 2R and ΔT_p is approximately $(T_{HPI} - T_m)$. Substituting the dimensionless boundary conditions into the balance equations in Table 1 yields the dimensionless balance equations in Table 2.

The dimensionless group Π_{QE} represents the ratio of the entrainment volumetric flux to the plume volumetric flux at the entrance. The dimensionless group, Fr_{HPI}, is the ratio of inertia to buoyancy and represents a modified Froude number. Here a_{HPI} is the cross-sectional flow area of the HPI nozzle. The dimensionless group, $\Pi_{\Delta T,}$ characterizes the degree of ambient thermal stratification. In conclusion, the dimensionless groups that govern the behavior of axisymmetric forced plumes in vertical flows are (D_{HPI}/z), Π_{QE}, Fr_{HPI}, and Π_{DT}.

Theofanous [15] and Rodi [14] have used a k-γ-θN turbulence model to predict the plume volumetric flow and temperature decay. Theofanous correlated the results of the more detailed analysis using the plume decay equations shown in Table 2. It is noted that these same dimensionless groups used in his correlation were also obtained in the present scaling analysis.

Table 1. Governing equations for a forced axisymmetric plume

Governing Balance Equations

Volume Balance:

$$\frac{dQ_p}{dz} = -\frac{dQ_E}{dz} \tag{20}$$

Momentum Balance:

$$\frac{d}{dz}\left(\frac{\rho Q_p^2}{b_u^2}\right) = 2\pi^2 g b_g^2 \left(\rho - \rho_L\right)_p \tag{21}$$

Energy Balance:

$$\frac{d}{dz}\left(\frac{Q_p \Delta T_p}{1+\lambda^2}\right) = -Q_p \frac{dT_m}{dz} \tag{22}$$

where λ is equal to b_u/b_g.

Initial and Boundary Conditions:

$$z^+ = \frac{2z}{D_{HPI}} \tag{23}$$

$$Q_p^+ = \frac{Q_p}{Q_{HPI}} \tag{24}$$

$$Q_E^+ = \frac{Q_E}{Q_{E,o}} \tag{25}$$

$$b_u^+ = \frac{2b_u}{D_{HPI}} \tag{26}$$

$$b_g^+ = \frac{2b_g}{D_{HPI}} \tag{27}$$

$$\Delta T_p^+ = \frac{\Delta T_p}{\left(T_{HPI} - T_m\right)} \tag{28}$$

$$\left(\frac{dT_m}{dz}\right)^+ = \left(\frac{dT_m}{dz}\right) \Big/ \left(\frac{dT_m}{dz}\right)_o \tag{29}$$

$$\Delta\rho_p^+ = \frac{\Delta\rho_p}{\left(\rho_{HPI} - \rho_m\right)} \tag{30}$$

Table 2. Dimensionless balance equations and Plume Decay Correlations

DIMENSIONLESS BALANCE EQUATIONS

Volume Balance:

$$\frac{dQ_p^+}{dz^+} = -\Pi_{QE}\frac{dQ_E^+}{dz^+} \tag{31}$$

Momentum Balance:

$$(Fr_{HPI})^2\frac{d}{dz^+}\left(\frac{\rho Q_p}{b_u^2}\right)^+ = 2\left(b_g^2\Delta\rho_p\right)^+ \tag{32}$$

Energy Balance:

$$\frac{d}{dz^+}\left(\frac{Q_p\Delta T_p}{1+\lambda^2}\right)^+ = -\frac{\Pi_{\Delta T}}{2}Q_p^+\left(\frac{dT_m}{dz}\right)^+ \tag{33}$$

DIMENSIONLESS GROUPS

$$\Pi_{QE} = \left(\frac{Q_E}{Q_{HPI}}\right)_o \tag{34}$$

$$Fr_{HPI} = \frac{Q_{HPI}}{a_{HPI}\left(\frac{g\Delta\rho_p D_{HPI}}{\rho_{HPI}}\right)_o^{1/2}} \tag{35}$$

$$\Pi_{\Delta T} = \frac{D_{HPI}}{(T_{HPI}-T_m)_o}\left(\frac{dT_m}{dz}\right)_o \tag{36}$$

PLUME DECAY CORRELATIONS (THEOFANOUS)

Entrainment Correlation:

$$\Pi_{QE} = 0.5176\left(\frac{z}{D_{HPI}}\right)^{1.236}(Fr_{HPI})^{-0.414} \tag{37}$$

Temperature Decay Correlation:

$$\Delta T^+ = 1-0.326\left(\frac{z}{D_{HPI}}\right)^{0.65}(Fr_{HPI})^{-0.274} \tag{38}$$

4.3. Governing equations for planar plumes

Chen and Rodi (1980) [13] have provided a valuable treatise which includes detailed discussions on planar plumes. The analysis for the planar plume follows that presented in Section 4.2 for the axisymmetric forced plume. The three fundamental assumptions, Taylor's entrainment assumption, the similarity of velocity and buoyancy profiles in the plume, and the Gaussian profile assumption remain applicable. Figure 17 illustrates the planar plume geometry.

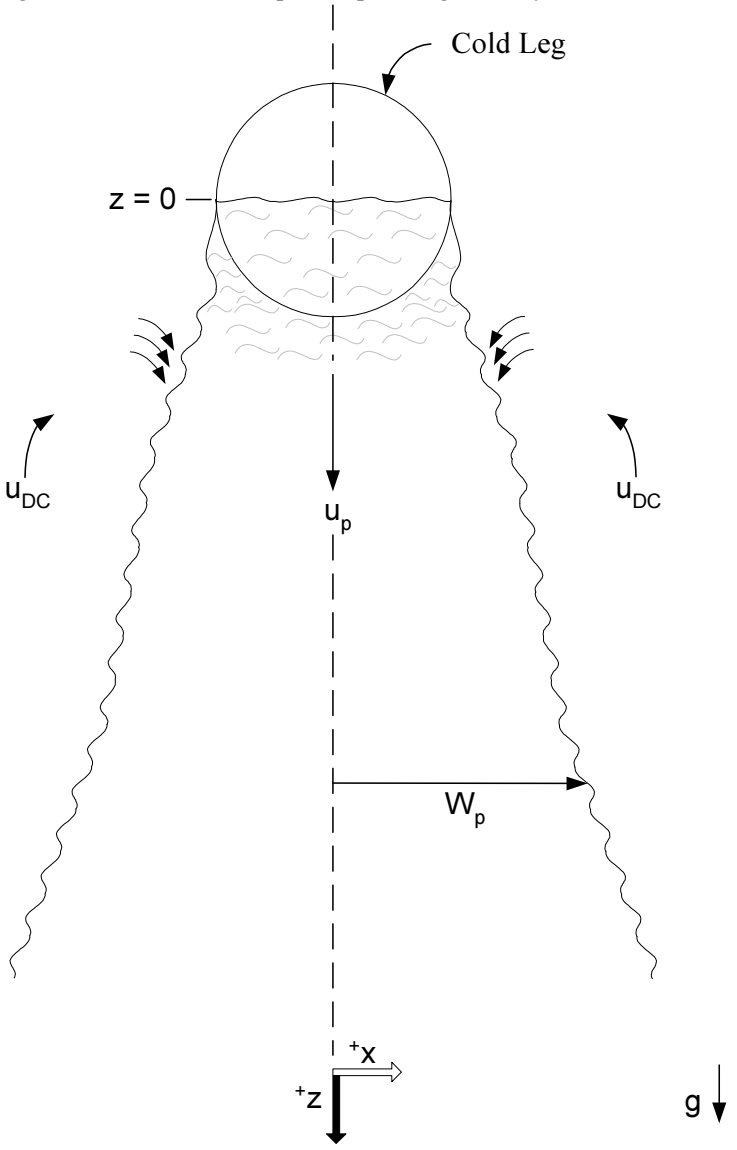

FIG. 17. Schematic of a single planar plume in the RPV downcomer.

The Gaussian profiles for the plume velocity, buoyancy and temperature are expressed as follows:

$$u(x,z) = u_p(z)\exp\left(-\frac{x^2}{b_u^2}\right) \tag{39}$$

$$g\Delta\rho(x,z) = g\Delta\rho_p(z)\exp\left(-\frac{x^2}{b_g^2}\right) \tag{40}$$

$$(T - T_m) = (T - T_m)_p \exp\left(-\frac{x^2}{b_g^2}\right) \tag{41}$$

The governing equations for the planar plume where gravity acts along the z-coordinate are (Chen and Rodi) [13]:

Mass Conservation:

$$\frac{\partial}{\partial z}(\rho u) + \frac{\partial}{\partial x}(\rho v) = 0 \tag{42}$$

Momentum Conservation:

$$\frac{\partial}{\partial z}(\rho u^2) + \frac{\partial}{\partial x}(\rho uv) = g(\rho - \rho_m) - \frac{\partial}{\partial x}(\rho u'v') \tag{43}$$

Thermal Energy:

$$\frac{\partial}{\partial z}[\rho u(T - T_m)] + \frac{\partial}{\partial x}[\rho v(T - T_m)] = -\rho u\frac{\partial T_m}{\partial x} - \frac{\partial}{\partial x}(\rho v'T') \tag{44}$$

where the definitions of the terms are the same as given in Section 4.2, and the thermal energy equation has been written in terms of the stratified ambient temperature, T_m. Integrating the equations over the cross-sectional area of the plume yields:

Volume Flux:

$$\frac{d}{dz}\int_0^{W_p} u\,dx = -v_E W_p \tag{45}$$

Momentum Flux:

$$\frac{d}{dz}\int_0^{W_p} \rho u^2\,dx = g\int_0^{W_p} (\rho - \rho_m)\,dx \tag{46}$$

Thermal Energy Flux:

$$\frac{d}{dz}\int_0^{W_p} u\left(T-T_m\right)dx = -\frac{dT_m}{dz}\int_0^{W_p} u dx \tag{47}$$

where ρ (Boussinesq approximation) and a factor of 2s were canceled from both sides of each equation and the plume boundary assumptions of Section 4.2 were applied. The downcomer gap width is denoted by "s."

Substituting the Gaussian profiles given by equations (39) through (41) into (45) through (47) respectively, yield the integral equations for the mean flow properties of the planar plume.

Volume Flux:

$$\frac{d}{dz}\left(b_u u_p\right) = -\frac{2}{\sqrt{\pi}} v_E \tag{48}$$

Momentum Flux:

$$\frac{d}{dz}\left(\rho b_u u_p^2\right) = 2g\Delta\rho_p b_g \tag{49}$$

Thermal Energy Flux:

$$\frac{d}{dz}\left[b_u u_p \Delta T_p \left(\frac{\lambda^2}{1+\lambda^2}\right)^{1/2}\right] = -b_u u_p \frac{dT_m}{dz} \tag{50}$$

The integral balance equations can be expressed in terms of volumetric flow rates as was done in Section 4.2. The volumetric flow rate of the plume, Q_p, is given by:

$$Q_P = 2s\int_0^{W_p} u dx \tag{51}$$

Substituting the Gaussian profile and integrating yields**:**

$$Q_p = \sqrt{\pi} b_u u_p s \tag{52}$$

The entrainment volumetric flow rate can be related to the entrainment velocity by:

$$\frac{dQ_E}{dz} = sW_p v_E \tag{53}$$

Substituting equations (52) and (53) into the integrated balance equation yields the governing balance equations for a planar plume. These equations are summarized in Table 3.

Table 3. Governing equations for planar plumes

Governing Balance Equations

Volume Balance:

$$\frac{dQ_p}{dz} = -\frac{dQ_E}{dz} \tag{20}$$

Momentum Balance:

$$\frac{d}{dz}\left(\frac{\rho Q_p^2}{b_u^2}\right) = 2\pi^2 s^2 g \Delta\rho_p b_g \tag{21}$$

Energy Balance:

$$\frac{d}{dz}\left(\frac{Q_p \Delta T_p \lambda}{\sqrt{1+\lambda^2}}\right) = -Q_p \frac{dT_m}{dz} \tag{22}$$

where λ is equal to b_u/b_g.

Initial and Boundary Conditions:

$$z^+ = \frac{2z}{D_{CL}} \tag{23}$$

$$Q_p^+ = \frac{Q_p}{Q_{po}} \tag{24}$$

$$Q_E^+ = \frac{Q_E}{Q_{E,o}} \tag{25}$$

$$b_u^+ = \frac{2b_u}{D_{CL}} \tag{26}$$

$$b_g^+ = \frac{2b_g}{D_{CL}} \tag{27}$$

$$\Delta T_p^+ = \frac{\Delta T_p}{\left(T_{po} - T_m\right)} \tag{28}$$

$$\left(\frac{dT_m}{dz}\right)^+ = \left(\frac{dT_m}{dz}\right) \Big/ \left(\frac{dT_m}{dz}\right)_o \tag{29}$$

$$\Delta\rho_p^+ = \frac{\Delta\rho_p}{\left(\rho_{po} - \rho_m\right)} \tag{30}$$

The initial half plume width, W_{po}, is assumed to be one half the cold leg diameter, D_{CL}. Substituting the dimensionless parameters into the integrated balance equations yields the dimensionless balance equations presented in Table 4. For uniform ambient fluid conditions in the downcomer, the fluid temperature gradient, dT_m/dz, would be zero.

Summarizing, the dimensionless groups that govern the behavior of the planar plume in the downcomer are (D_{CL}/z), Π_{QE}, Fr_{DC}, and $\Pi_{\Delta T}$.

Table 4. Dimensionless balance equations for planar plumes

DIMENSIONLESS BALANCE EQUATIONS

Volume Balance:

$$\frac{dQ_p^+}{dz^+} = -\Pi_{QE}\frac{dQ_E^+}{dz^+} \tag{31}$$

Momentum Balance:

$$\left(Fr_{DC}\right)^2\frac{d}{dz^+}\left(\frac{\rho Q_p}{b_u^2}\right)^+ = \frac{\pi}{2}\Delta\rho_p^+ b_g^+ \tag{32}$$

Energy Balance:

$$\frac{d}{dz^+}\left(\frac{Q_p\Delta T_p\lambda}{\sqrt{1+\lambda^2}}\right)^+ = -\frac{\Pi_{\Delta T}}{2}Q_p^+\left(\frac{dT_m}{dz}\right)^+ \tag{33}$$

DIMENSIONLESS GROUPS

$$\Pi_{QE} = \left(\frac{Q_E}{Q_p}\right)_o \tag{34}$$

$$Fr_{DC} = \frac{Q_{p,o}}{sD_{CL}\left(\dfrac{g\Delta\rho_p D_{CL}}{\rho_p}\right)_o^{1/2}} \tag{35}$$

$$\Pi_{\Delta T} = \frac{D_{CL}}{\left(T_p - T_m\right)_o}\left(\frac{dT_m}{dz}\right)_o \tag{36}$$

PLANAR PLUME VELOCITY AND HEAT TRANSFER

Plume Velocity Correlation (Kotsovinos):

$$u_p = 1.66\left(\frac{Q_{p,o}g\left(\rho_{HPI} - \rho_m\right)}{s\rho_m}\right)^{1/3} \tag{37}$$

Dimensionless Plume Velocity:

$$u_p^+ = \frac{u_p sD_{CL}}{Q_{p,o}} = 1.66\left(\frac{\rho_p}{\rho_m}\right)^{1/3}\left(Fr_{DC}\right)^{-2/3} \tag{38}$$

$$Nu_p = C\cdot \mathrm{Re}_p^{0.8}\,\mathrm{Pr}^{0.4} \tag{39}$$

$Nu_p = \dfrac{2sh_p}{k_f}$ **(40)**	$\mathrm{Re}_p = \dfrac{2u_p s}{\nu_f}$ **(41)**	$\mathrm{Pr} = \dfrac{c_p\mu_f}{k_f}$ **(42)**

Table 4 also includes correlations for the mean planar plume velocity and planar plume convective heat transfer. The correlation presented in Table 4 was adapted from the work of Kotsovinos [16] to predict the mean fluid velocity at the axis of a plume.

Valenzuela and Dolan used the well-known Dittus-Boelter correlation for turbulent flow to predict the plume heat transfer coefficients in the CREARE 1/2-Scale test facility [5]. However, the Reynolds number and Prandtl Number have been expressed in terms of the plume velocity, u_p. Figure 18 shows the comparison of this equation to the CREARE 1/2- scale data. The data collapse quite neatly to a single line.

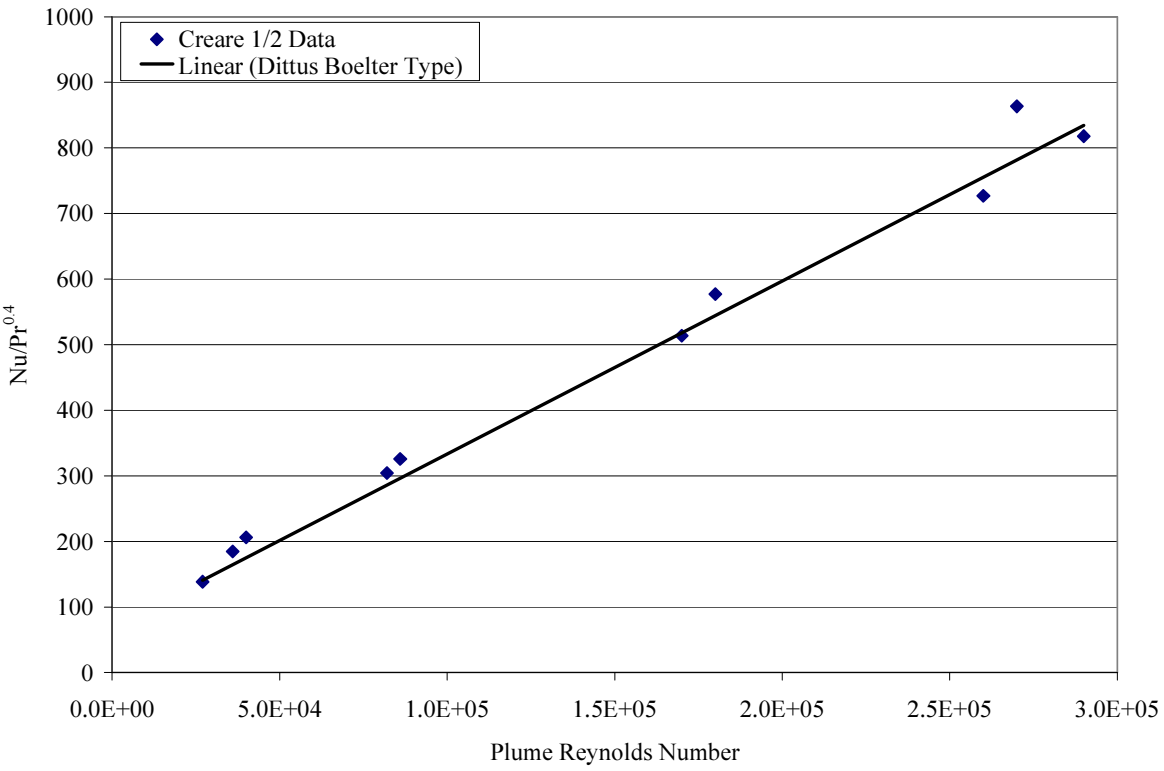

FIG. 18. Comparison of plume heat transfer correlation predictions to the Creare 1/2-Scale Downcomer Heat Transfer Data.

4.4. Downcomer plume behavior

Flow visualization tests examining downcomer plume behavior were obtained from the 2/5 scale, multi-loop, transparent test facility at Imatran Voima Oy (IVO) in Helsinki, Finland [17]. Figure 19 presents two snapshots of IVO Test #102 showing plume penetration into the downcomer and the resulting thermal stratification that arises. Dense HPI fluid flows through Cold Leg B as indicated by the dye, while a loop flow rate 10 times greater flows through Cold Leg C.

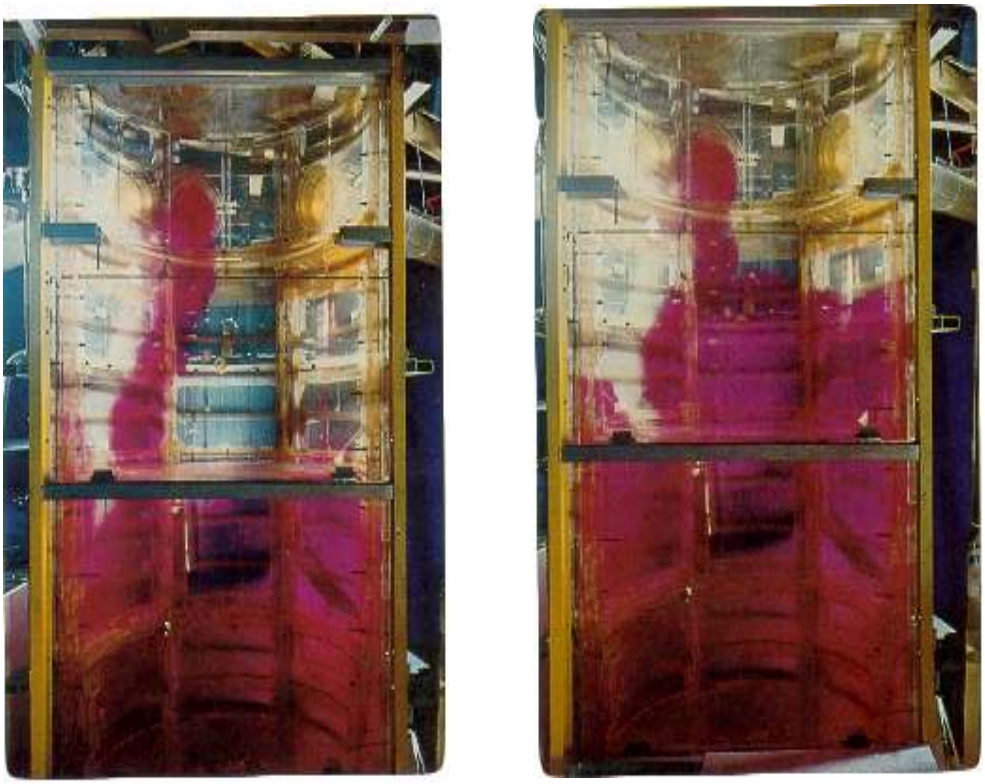

FIG. 19. Photographs of the IVO transparent test loop. Cold Leg C flow rate = 66 gpm (4.2 liters/s) and HPI flow in Cold Leg B = 6.6 gpm (0.42 liters/s).

Plume interactions, similar to those observed in the IVO test loop were also measured in the APEX-CE tests. Figure 20 is a schematic of planar plumes generated by two cold legs merging to form a stronger central plume. The complexity of the behavior, in particular the interactions between plumes, does not lend itself to simple analysis.

Researchers at Purdue and University of California, Santa Barbara developed a regional mixing model called REMIX [18] to assess thermal fluid mixing behavior in the HPI line, cold leg and downcomer or a PWR. Assessments of REMIX using APEX-CE thermal data indicate that the model typically predicts lower temperatures than measured. The code is limited however, in that it cannot model multiple plume interactions.

A variety of Computational Fluid Dynamics (CFD) codes have been used to examine fluid mixing in reactor vessels. STAR-CD, CFX, and FLUENT are examples of commercially available codes that offer promising methods for analyzing the complex mixing behavior produced by nuclear reactor safety injection systems. This topic will be discussed in a separate lecture**.**

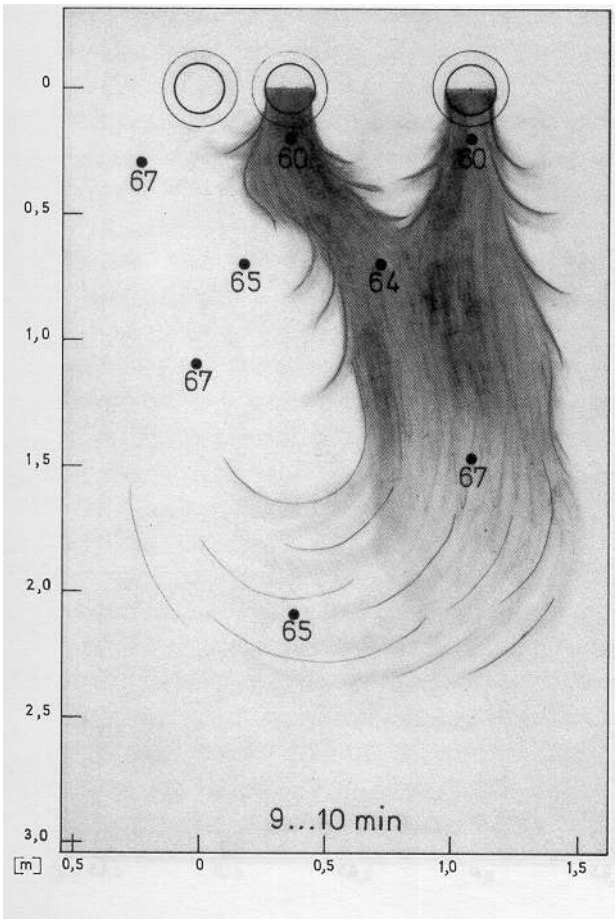

FIG. 20. Downcomer plume interactions as observed in IVO 2/5 scale transparent test loop (IVO Mixing Test #115).

NOMENCLATURE

Fr_x –Froude Number Modified (HPI or HPI/CL)
Q – Volumetric flow rate
g - gravitational constant
a – cross-sectional flow area
D – Diameter
ρ - density
v_E – Entrainment velocity
α_E – Entrainment constant
u – velocity
T – Temperature
R – Radial coordinate
b_u – Empirically determined constant for radial spread of velocity profile
b_g - Empirically determined constant for radial spread of buoyancy profile
β_o - Reference thermal expansion coefficient
z – Axial Coordinate
R – Plume radius
W – Plume Half-width
s – Downcomer gap size

ACKNOWLEDGEMENT

This work was supported through a U.S. Department of Energy Contract (DE- FC07-04ID14550) and the Oregon State University sabbatical program. This work was conducted through the IAEA Nuclear Power Technology Development Section.

REFERENCES

[1] LOOMIS, G.G., and SODA, K., Results of the Semiscale MOD-2A Natural Circulation Experiments, U. S. Nuclear Regulatory Commission, NUREG/CR-2335 (1982).

[2] THEOFANOUS, T.G., NOURBAKHSH, H.P., GHERSON, P., and IYER, K., Decay of Buoyancy Driven Stratified Layers with Applications to Pressurized Thermal Shock (PTS), U.S. Nuclear Regulatory Commission, NUREG/CR-3700, May 1984.

[3] REYES, J.N., JR., A transition criterion for the onset of slugging or mixing in horizontal conduits, experimental heat transfer, fluid mechanics, and thermodynamics 2001, Eddizoni ETS Pisa Italy, Volume II-1477 (2001).

[4] FANNING, M.W. and ROTHE, P.H., *Transient Cooldown in Model Cold Leg and Downcomer, Electric Power Research Institute,* Interim Report EPRI NP-3118, May 1983.

[5] VALENZUELA, J.A. and DOLAN, F.X., Thermal and Fluid Mixing in a 1/2 –Scale Test Facility, U.S. Nuclear Regulatory Commission, NUREG/CR-3426, September 1985.

[6] THEOFANOUS, T.G., IYER, K., NOURBAKHSH, H.P., and GHERSON, P., Buoyancy effects of overcooling transients calculated for the NRC pressurized thermal shock study, driven stratified layers with applications to pressurized thermal shock (PTS), U.S. Nuclear Regulatory Commission, NUREG/CR-3702, May 1986.

[7] ROUSE, H., YIH, C.S. and HUMPHREYS, H.W., Gravitational convection from a boundary source, *Tellus*, Vol. 4, pp. 201-210 (1952).

[8] BATCHELOR, G.K., Heat convection and buoyancy effects in fluids, *Quarterly Journal of the Royal Meteorological Society*, Vol. 80, pp. 339-358 (1954).

[9] MORTON, B.R., Forced plumes, *Journal of Fluid Mechanics*, Vol. 5, pp. 151-163 (1959).

[10] TURNER, J.S., Buoyancy effects in fluids, Cambridge University Press, Cambridge (1979).

[11] MORTON, B.R., TAYLOR SIR G. and TURNER, J.S., Turbulent gravitational convection from maintained and instantaneous sources, *Proceedings of the Royal Society*, A 234, pp. 1-23 (1956).

[12] FOERTHAMNN, E., Turbulent jet expansion, English Translation, A.C.A. TM-789, (Original paper in German, 1934, Ing. Archiv., 5) 1934. (Reproduced by N.P. Cheremisinoff, Editor, Dynamics of Single-Fluid Flows and Mixing, *Encyclopedia of Fluid Mechanics*, Vol. 2,, Gulf Publishing Company, Houston (1986).

[13] CHEN, C.J., and RODI, W., *Vertical Turbulent Buoyant Jets- A Review of Experimental Data*, *HMT*, Vol. 4, Pergamon Press, New York (1980).

[14] RODI, W., *Turbulent Buoyant Jets and Plumes, HMT*, Vol. 6, Pergamon Press, New York (1982).

[15] THEOPFANOUS, T.G., ANGELINI, S, and YAN, H., Universal Treatment of Plumes and Stresses for Pressurized Thermal Shock Evaluations, U.S. Nuclear Regulatory Commission, NUREG/CR-5854, June 1982.

[16] KOTSOVINOS, N.E., Plane turbulent buoyant jets, Ph.D. Thesis, California Institute of Technology (1975).

[17] TUOMISTO, H., and P. MUSTONEN. Thermal Mixing Tests in a Semiannular Downcomer with Interacting Flows from Cold Legs, U.S. Nuclear Regulatory Commission, NUREG/IA-0004, October 1986.

[18] IYER, K. NOURBAKHSH, H.P. and THEOFANOUS, T.G., REMIX: A computer program for temperature transients due to high pressure injection after interruption of natural circulation, Purdue University, U.S. Nuclear Regulatory Commission, NUREG/CR-3701, May 1986.